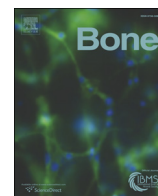| Title	Trabecular health of vertebrae based on anisotropy in trabecular architecture and collagen/apatite micro-arrangement after implantation of intervertebral fusion cages in the sheep spine
Author(s)	Ishimoto, Takuya; Yamada, Katsuhisa; Takahashi, Hiroyuki et al.
Citation	Bone. 2018, 108, p. 25-33
Version Type	VoR
URL	https://hdl.handle.net/11094/89831
rights	This article is licensed under a Creative Commons Attribution 4.0 International License.
Note	

Full Length Article

Trabecular health of vertebrae based on anisotropy in trabecular architecture and collagen/apatite micro-arrangement after implantation of intervertebral fusion cages in the sheep spine

Takuya Ishimoto [a], Katsuhisa Yamada [b], Hiroyuki Takahashi [a,c], Masahiko Takahata [b], Manabu Ito [d], Takao Hanawa [e], Takayoshi Nakano [a,*]

[a] Division of Materials and Manufacturing Science, Graduate School of Engineering, Osaka University, 2-1, Yamada-Oka, Suita, Osaka 565-0871, Japan
[b] Department of Orthopedic Surgery, Graduate School of Medicine, Hokkaido University, North-15, West-7, Kita-ku, Sapporo, Hokkaido 060-8638, Japan
[c] Teijin Nakashima Medical Co., Ltd., 688-1 Joto-Kitagata, Higashi-ku, Okayama 709-0625, Japan
[d] Department of Spine and Spinal Cord Disorders, National Hospital Organization, Hokkaido Medical Center, 5-7-1-1 Yamanote, Nishi-ku, Sapporo, Hokkaido 063-0005, Japan
[e] Institute of Biomaterials and Bioengineering, Tokyo Medical and Dental University, Kanda-surugadai, Chiyoda-ku, Tokyo 101-0062, Japan

ARTICLE INFO

ABSTRACT

Healthy trabecular bone shows highly anisotropic trabecular architecture and the preferential orientation of collagen and apatite inside a trabecula, both of which are predominantly directed along the cephalocaudal axis. This makes trabecular bone stiff in the principally loaded direction (cephalocaudal axis). However, changes in these anisotropic trabecular characteristics after the insertion of implant devices remain unclear. We defined the trabecular architectural anisotropy and the preferential orientation of collagen and apatite as parameters of trabecular bone health. In the present study, we analyzed these parameters after the implantation of two types of intervertebral fusion cages, open and closed box-type cages, into sheep spines for 2 and 4 months. Alteration and evolution of trabecular health around and inside the cages depended on the cage type and implantation duration. At the boundary region, the values of trabecular architectural anisotropy and apatite orientation for the closed-type cages were similar to those for isotropic conditions. In contrast, significantly larger anisotropy was found for open-type cages, indicating that the open-type cage tended to maintain trabecular anisotropy. Inside the open-type cage, trabecular architectural anisotropy and apatite orientation significantly increased with time after implantation. Assessing trabecular anisotropy might be useful for the evaluation of trabecular health and the validation and refinement of implant designs.

1. Introduction

The evaluation of bone health, including structural and functional soundness, after the implantation of bone joint devices is crucial for validating and improving them. The spine plays significant functional roles, such as load bearing and hematopoiesis; therefore, devices for the spine, such as intervertebral fusion cages and pedicle screws, should be created to facilitate the maintenance and quick recovery of spinal function.

The spine is predominantly longitudinally loaded [1]. Vertebral bodies consisting of a cortical shell and inner trabecular bone mainly play the role of sustaining the load applied to the spine [2]. The stress field in the vertebral body is highly anisotropic; it is almost uniaxial along the cephalocaudal axis [1,3]. Likewise, the mechanical property of the vertebral body is anisotropic [4]. The mechanical properties of biological materials including bone are often based on their macroscopic

architecture and the specific arrangement of their microstructure [5]. Hierarchical ordering is effectively used in many biological materials to maximize their functionality. With regard to trabecular bone, which was reported to contribute to a significant proportion of vertebral strength [6–8], hierarchically ordered anisotropic structuring sustains the anisotropic stress field. The macroscopic trabecular architectural orientation predominantly runs along the principal stress line, which is typically seen in the proximal femur [9], calcaneal bone [10], and vertebral body [11,12]; this is known as Wolff's law. As a result, trabecular bone exhibits macroscopic anisotropy in an apparent Young's modulus [12,13]. In addition, trabeculae show anisotropy in their component material, which mainly comprises organic collagen fibers and inorganic apatite crystals. In a trabecula, the crystallographic c-axes of apatite [14, 15] and collagen molecules [16], which act as templates for the epitaxial precipitation of apatite, are preferentially oriented parallel to the trabecular long axis. The apatite c-axis and collagen fiber direction (the stronger direction of each material) co-orient in the trabecular direction, leading to anisotropy of the intrinsic mechanical property such that

* Corresponding author.
E-mail address: nakano@mat.eng.osaka-u.ac.jp (T. Nakano).

the Young's modulus measured along the trabecular axis is greater than that along the transverse axis [17]. Thus, trabecular bone is efficiently strengthened in the principally-loaded direction through the formation of hierarchical anisotropy in structure and mechanical properties.

The preferential orientation of collagen and the apatite *c*-axis is of recent interest as a bone quality index because of its importance in evaluating and predicting the mechanical properties and anisotropy of bone [18–20]. It is becoming an important parameter for developing implant devices in accordance with the concept that an implant should not disrupt the structure of surrounding bone tissue and should generate bone with an optimally oriented microstructure [21,22]. However, the effect of implant devices on the orientation of the trabecular structure remains unclear. In the present study, two types of intervertebral fusion cage were investigated. One is a widely used, open box-type cage with a large cavity for the bone graft to promote fusion between the vertebral bodies. The other is a closed box-type cage that was recently introduced to eliminate the need for an autogenous iliac bone graft [23,24]. The bonding strength at the bone-cage interface was reported to differ between the two cages [23], suggesting a difference in bone formation behavior around them.

Here, we defined the anisotropic features of trabecular bone, i.e., trabecular architectural anisotropy and preferential orientation of collagen and apatite, as parameters for trabecular bone health. We analyzed such parameters after the implantation of two different intervertebral fusion cages into the spines of sheep. The aims of the present study were to compare the health of the trabecular bone surrounding the two types of cage and to trace the evolution of trabecular anisotropy over time in the cavity of the open-type cage. The findings of this study demonstrate the importance of assessing trabecular anisotropy as a parameter of bone health for the validation and optimization of implant design.

2. Materials and methods

2.1. Intervertebral fusion cages

Closed-type (Fig. 1a) and open-type (Fig. 1b) intervertebral fusion cages with dimensions of $8 \times 8 \times 20$ mm were prepared. For the closed cage, a 1-mm thick porous titanium (Ti) sheet was firmly attached to the upper, lower (5×13 mm), and lateral surfaces (5×6 mm) of the cage by a diffusion bonding method to enhance the compatibility with trabecular bone [23]. The porous Ti sheet was prepared with a porosity of 80% using the slurry foaming method [25]. The open-type cage had a large cavity (5×13 mm) that encompassed the middle of the cage. The open cage and the main body of the closed-type cage were shaped by machining.

2.2. Sheep animal model and surgical operation

This animal study was conducted in accordance with the Guidelines for Proper Conduct of Animal Experiments established by the Science
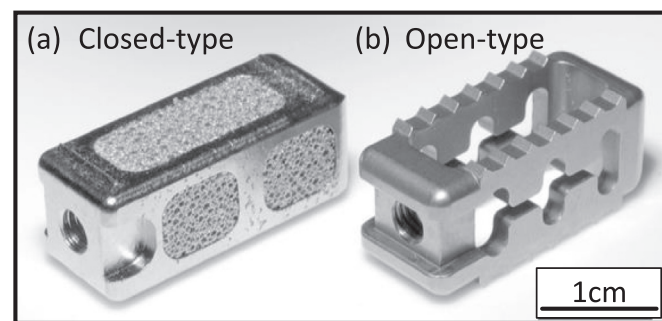

Fig. 1. Two-types of intervertebral fusion cages with dimensions of $8 \times 8 \times 20$ mm. (a) Closed-type titanium (Ti) cage with a porous Ti sheet on its surfaces. (b) Open-type Ti-6Al-4V cage with a large cavity (5×13 mm).

Council of Japan. This study was approved by the Institutional Review Board of the Bioscience Department/Toya Laboratory of Hokudo Co., Ltd. We used twelve adult male Suffolk sheep, approximately 20 months of age and weighing about 45 kg. Closed-type and open-type intervertebral fusion cages were randomly placed at the L2–3 or L4–5 disc levels.

An anterior lumbar interbody fusion was performed on each animal through a right retroperitoneal approach under general anesthesia as previously described [26]. After total removal of the L2–3 and L4–5 intervertebral discs and the upper and lower cartilage endplates, a cage was inserted into these spaces. The space for cage insertion was about 9 mm. An 8-mm cage height would be appropriate for this animal model without causing significant destruction to the bony endplates. After placement of the cages, a single screw/rod system consisting of 5-mm diameter screws (Kaneda SR, Depuy Synthes Spine, Raynham, MA, USA) was applied across L2–3 and L4–5 to afford immediate stability over the surgical sites. An autogenous iliac bone graft taken from the right iliac crest of the same animal was packed inside the open-type cage. According to the recommendation of time points for bone analysis in the sheep cage model by Lindley et al. [27], six sheep were euthanized at 2 months and the remaining six at 4 months using bolus intravenous injections of pentobarbital sodium and the lumbar spines, including the cages, were removed.

2.3. Analysis of the degree of anisotropy (DA) of trabecular bone architecture

Bone specimens of 1-mm thickness were sectioned along the sagittal plane with a diamond band saw system (BS-300CP; Exakt Apparatebau, Germany). Micro-computed tomography (μCT) was operated at 35 kV and 25 μA to produce bone images with a spatial resolution of 12 μm on each side to analyze the architectural anisotropy of vertebral trabecular bone. For binarization of the μCT image, a threshold value was determined as follows. A histogram curve for the gray value derived from the μCT image with two peaks from bone and other tissues was fitted by summing two normal distribution functions. The gray value located corresponding to the upper 70% of the area under the fitted curve for bone was used as a threshold for binarization. In the sagittal image, distant, boundary, and inner regions with dimensions of 3×3 mm were defined (see Figs. 2 and 5). The bone volume fraction, defined as bone volume/total volume of interest (BV/TV), was determined. The fabric ellipse of the mean intercept length was calculated from the bone architecture in the sagittal plane [28]. DA of trabecular bone was determined two-dimensionally (2D) as the aspect ratio (major axis length/minor axis length) of the fabric ellipse and the angle of the long axis of the ellipse from the cephalocaudal axis was obtained. For these analyses, TRI/3D-BON software (Ratoc System Engineering, Japan) was used.

2.4. Analysis of apatite c-axis orientation

A 1-mm-thick section, identical to that used for μCT analysis, was used for analyzing the preferential orientation of the apatite *c*-axis. A microbeam X-ray diffractometer with a transmission optical system (R-Axis BQ; Rigaku, Japan) was used. Mo–Kα radiation was generated at 50 kV and 90 mA. The incident beam was collimated into an 800-μm circular spot using a double-pinhole metal collimator and projected vertically onto the specimen to analyze the 2D distribution of the apatite *c*-axis orientation along the surface of the thin specimen. The diffracted X-rays were collected by an imaging plate placed behind the specimen. The diffracted beam was collected for 900 s.

From the Debye ring, the diffraction intensities (I) of the (002) and (310) planes of the biological apatite were integrated along the azimuthal angle (β) at steps of 1°. The (002) crystal plane is representative of the apatite *c*-axis and the (310) plane is orthogonal to the (002) plane. Intensity distributions ($I(\beta)$) as a function of β for the diffraction intensities of the (002) and (310) planes ($I_{002}(\beta)$ and $I_{310}(\beta)$) were
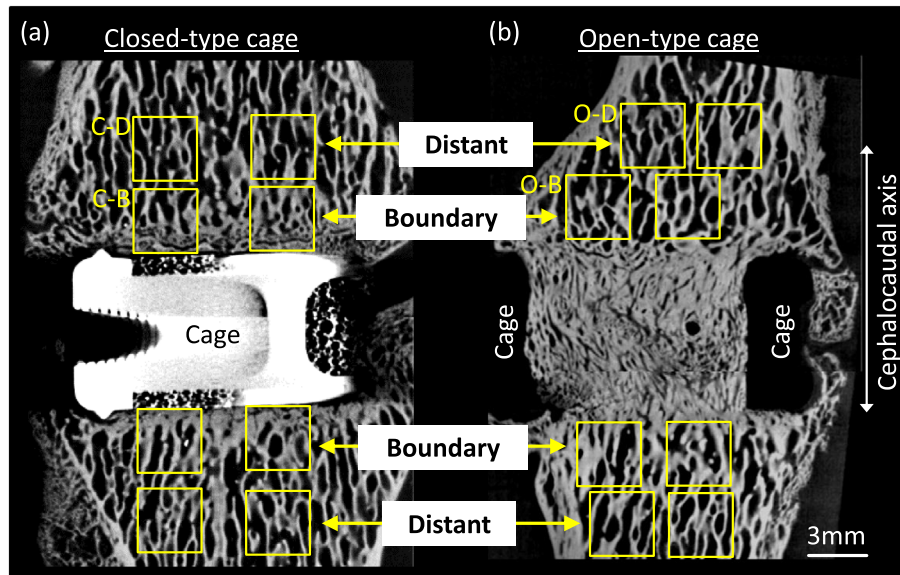
Fig. 2. Sagittal micro-CT (μCT) images of sheep vertebral bodies implanted with (a) closed- and (b) open-type intervertebral fusion cages at 2 months after surgery. C-D: Distant region for the closed-type cage; C-B: Boundary region for the closed-type cage; O-D: Distant region for the open-type cage; O-B: Boundary region for open-type cage.

individually fitted using the following elliptic polynomial function (subtracted by a constant d) to minimize the effects of data scattering using the least-squares method [21]:

$$I(\beta) = \left\{ \frac{\cos^2(\beta-\mu)}{a^2} - \frac{\sin^2(\beta-\mu)}{b^2} \right\}^{\frac{1}{2}} - d$$

In this equation, a, b, d, and μ are the fitting parameters and μ is the angle at which the intensity peaks. Finally, the degree of the apatite c-axis orientation was calculated for each β as the ratio of (002) intensity to (310) intensity $\left(\frac{I_{002}(\beta)}{I_{310}(\beta)}\right)$, resulting in 2D apatite c-axis orientation as a function of β along the plane vertical to the incident X-ray beam. Randomly-oriented hydroxyapatite powder provided by the National Institute of Standards and Technology (NIST) (product #2910: calcium hydroxyapatite) showed an intensity ratio of 0.6; therefore, values over 0.6 indicated the presence of preferential apatite c-axis orientation in the analyzed direction. The 2D distribution of apatite orientation was expressed as a polar diagram and the maximum value was used for analysis.

2.5. Histology and analysis of collagen orientation

Another sagittal section was prepared for undecalcified staining. The specimen was sectioned using the aforementioned diamond band saw system into an appropriate thickness and was then ground to 0.1-mm thickness. Staining with hematoxylin & eosin and toluidine blue O was performed. Histological images and polarized images were taken with an optical microscope (BX60; Olympus, Japan). A 2D birefringence analyzer (WPA-micro, Photonic Lattice, Japan) was utilized to assess collagen orientation in the sagittal plane. For birefringence analysis, three polarized monochromatic lights with wavelengths of 523, 543, and 575 nm were used, along with $5\times$ and $10\times$ objective lenses. Since collagen is a positively birefringent material [29], the optical fast and slow axes lie orthogonal and parallel to the long axis of the collagen fibers [30]; therefore, we analyzed the slow-axis direction for preferential collagen orientation.

2.6. Statistical analyses

Quantitative results were expressed as the mean ± standard deviation. Statistical significance was determined using either two-tailed t-test (paired or unpaired) or analysis of variance (ANOVA) with variances of cage type, implantation duration, region, or combinations of them. Post hoc Tukey HSD comparisons were conducted, where appropriate. A P-value < 0.05 was considered statistically significant. SPSS version 14.0J software (SPSS Japan Inc., Japan) for Microsoft Windows was used for the statistical analyses.

3. Results

3.1. Comparison of trabecular anisotropy around the cage: closed vs. open-type cages

Fig. 2 shows the sagittal μCT images of sheep vertebral bodies implanted with intervertebral fusion cages at 2 months after surgery. Bony fusion was achieved through the large cavity inside the open-type cage. The DA of trabecular bone and the degree of apatite c-axis orientation were analyzed in the boxed regions (3×3 mm), which were defined as distant and boundary regions.

Typical fabric ellipses and polar diagrams representing trabecular structural anisotropy and distribution of apatite c-axis orientation, respectively, are shown in Fig. 3. Essentially, the directions of the trabecular architecture and apatite c-axis preferentially oriented along the cephalocaudal axis. The boundary region for the closed-type cage (C-B) showed more isotropic features. Fig. 4a and b compares the DA of trabecular bone and the degree of apatite c-axis orientation between the two types of cages. For both, the boundary region for the closed-type cage shows significantly lower anisotropy ($P < 0.01$ and $P = 0.012$, respectively). Fig. 4c–e shows histology and collagen orientation around the bone/implant interface for the closed-type cage with a porous titanium layer on its surface. Active bone ingrowth into pores was observed; however, patchy contrast seen around the interface in polarized and birefringence images (Fig. 4d–e) indicated randomly organized collagen microstructure, while elongated trabeculae apart from the cage surface (seen on the left side of Fig. 4c–e) showed well-organized and aligned collagen along the trabecular direction (see arrows in Fig. 4e). The less anisotropic trabecular features at the boundary region continued until 4 months (data not shown).

3.2. Evolution of bone structure over time after insertion of the open-type cage

3.2.1. Bone volume fraction (BV/TV)

Fig. 5 shows the sagittal μCT images of vertebral bodies implanted with the open-type intervertebral fusion cages at 2 and 4 months after
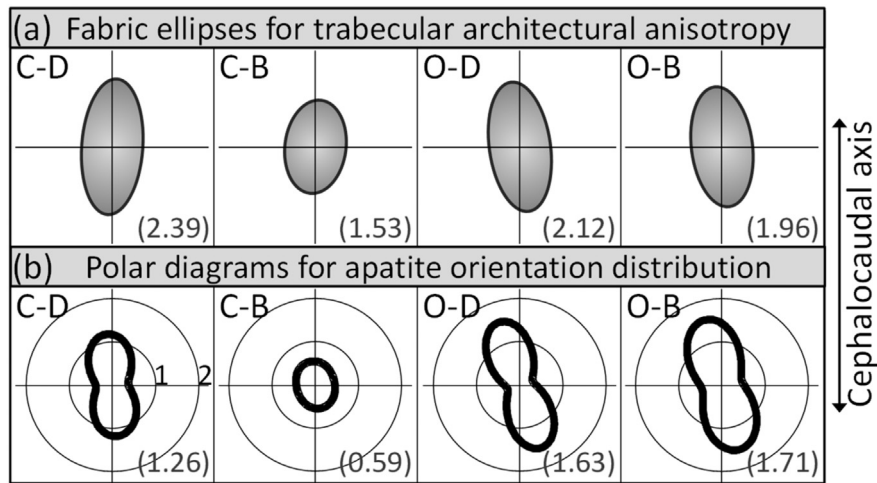
Fig. 3. Anisotropic features of trabecular bone at distant and boundary regions for the two-types of cages. (a) Typical fabric ellipses representing 2D trabecular architectural anisotropy in the sagittal plane. Minor axis length of fabric ellipses was normalized. (b) Polar diagrams representing 2D distribution of the apatite orientation in the sagittal plane. The radius represents the degree of apatite *c*-axis orientation. Values in brackets correspond to the major axis length of each shape. The larger values represent the more prominent anisotropy.

surgery. At 2 months, the autogenous iliac bone graft was replaced with newly formed bone in the inner region. As shown in Fig. 6, BV/TV of the inner region was significantly higher ($P < 0.01$) than that of the distant region at 2 months after surgery. It decreased significantly ($P < 0.01$) until 4 months after surgery; however, it was still higher ($P < 0.01$) than that of the distant region at 4 months.
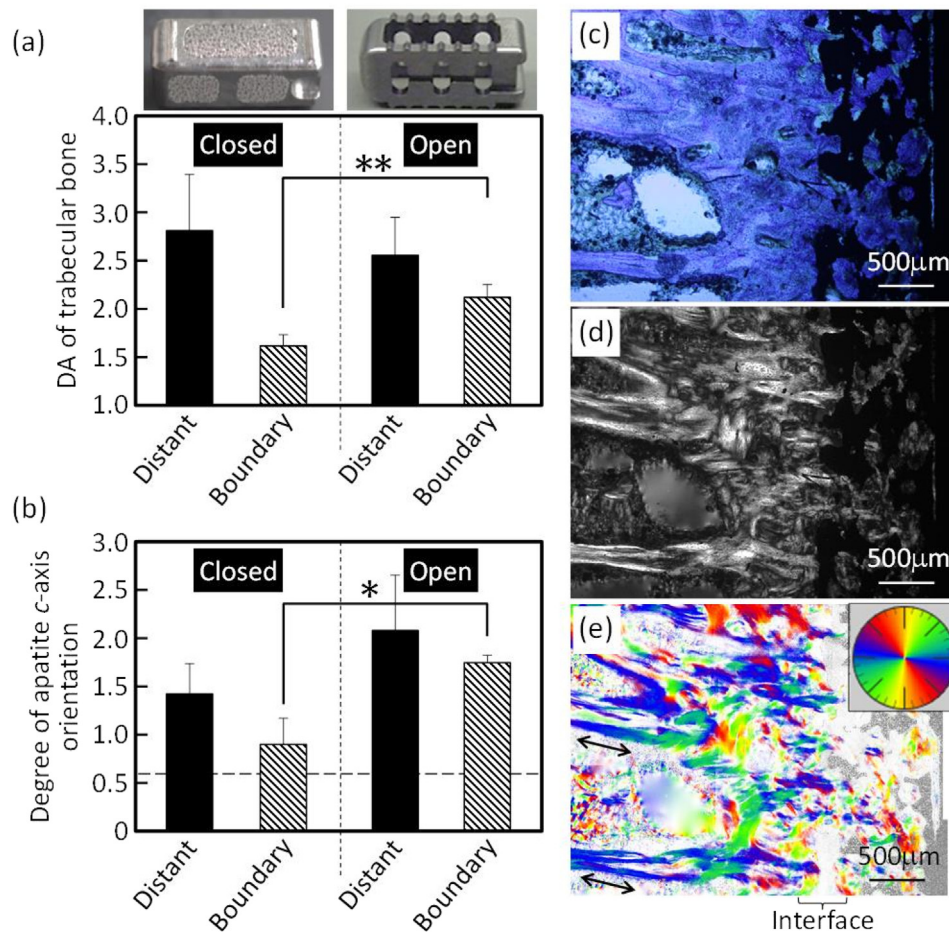

Fig. 4. Comparison of trabecular anisotropy between the closed- and open-type cages, and less-organized collagen arrangement at the interface of bone and porous coating of the closed-type cage. (a) The degree of anisotropy (DA) of the trabecular structure and (b) the degree of preferential apatite *c*-axis orientation. Value for a random apatite orientation is equal to 0.6. (c) Optical microscope images of the sagittal section stained with hematoxylin & eosin and toluidine blue O around the bone-closed-type cage interface, (d) the corresponding polarized image, and (e) birefringence images. Color indication at the right-top of (e) shows the slow-axis direction of birefringence representing the preferential collagen orientation direction. Regions showing very small retardance were pale- or white-colored. *$P < 0.05$, **$P < 0.01$ by paired *t*-test.

3.2.2. Trabecular architectural anisotropy and apatite orientation

Fig. 7 shows the variation of the DA of trabecular bone architecture and the angular difference between the trabecular direction (direction of the major axis of the fabric ellipse) and the cephalocaudal axis. At 2 months, the trabecular architecture of the inner region was nearly isotropic (DA was approximately 1). At 4 months, the DA significantly increased ($P = 0.016$) and the angular difference significantly dropped ($P = 0.018$) to a lower value in the inner region, which showed that the trabecular bone developed anisotropic morphology along the cephalocaudal axis.

Fig. 8 shows the variation of the degree of apatite c-axis orientation. At 2 months, the apatite orientation of the inner region was significantly lower ($P = 0.025$) than that of the distant region; it significantly increased ($P = 0.028$) until 4 months.

3.2.3. Histology and collagen orientation in the inner region

Histology, polarized imaging, and birefringence property are shown in Fig. 9. At 2 months, immature woven-type bone (Fig. 9a) with no specific directionality of collagen was seen (Fig. 9c, e) in the inner region of the cage. Osteocytes (arrowheads) in this bone were randomly distributed (Fig. 9a). The immature bone was replaced by a rod-like trabecular bone, which preferentially aligned along the cephalocaudal axis, by 4 months through remodeling (Fig. 9b). In a trabecula, collagen preferentially and homogeneously oriented parallel to the trabecular direction (cephalocaudal axis) (Fig. 9d, f), and osteocytes elongated and aligned in the same direction (Fig. 9b). Taken together with the apatite orientation, collagen and apatite c-axis preferentially oriented along the cephalocaudal axis at 4 months after surgery, as illustrated in Fig. 9(g), which might be approaching the microstructural features of a healthy trabecula. However, it may have required more time to fully recover trabecular health in the inner region.

4. Discussion

The present study investigated the change in vertebral trabecular anisotropy at two length-scale levels (trabecular architectural anisotropy and micro-arrangement of apatite and collagen inside the trabeculae) after the implantation of two types of intervertebral fusion cage. Alteration and evolution of trabecular health around and inside the implants were observed.
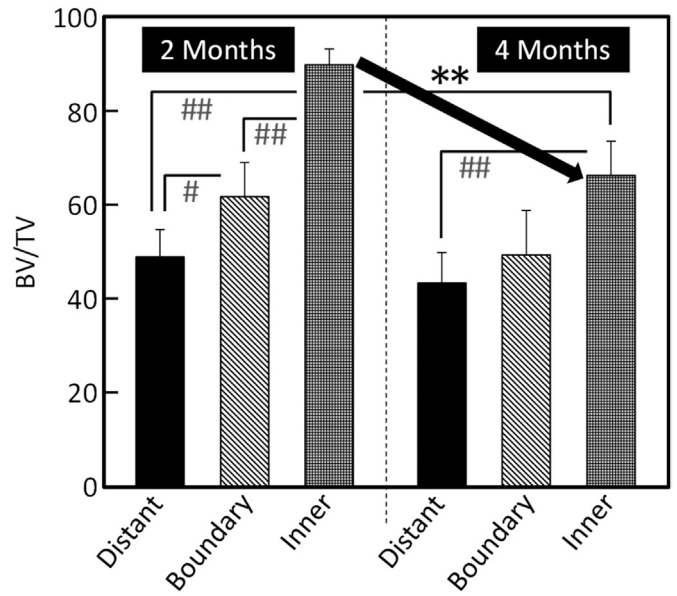

Fig. 6. Sagittal μCT images of sheep vertebral bodies implanted with the open-type intervertebral fusion cages at (a) 2 and (b) 4 months after surgery. **$P < 0.01$ by unpaired t-test. #$P < 0.05$, ##$P < 0.01$ by Tukey HSD test.

4.1. Validity of the sheep model

The validity of the sheep model for the study of the spine and spinal devices from the biomechanical viewpoint should be discussed. A major difference between biped humans and quadruped sheep is the direction of the spine axis, which is vertical in humans and horizontal in quadruped animals. However, the sheep spine has been reported to show similarities with the human spine in its geometry [31], mechanical properties [32], and most importantly, the anisotropy of lumbar trabecular bone [3]. A report from Wang et al. [3] clearly stated that the trabeculae preferentially run parallel to the cephalocaudal axis in the lumbar vertebrae of both humans and sheep, which substantiates, according to Wolff's law, that the vertebral bodies are mainly loaded along the cephalocaudal axis in sheep and humans. Biped and quadruped spines are substantially loaded in a similar manner. As such, the sheep model is useful for the research of spinal devices for use in humans.
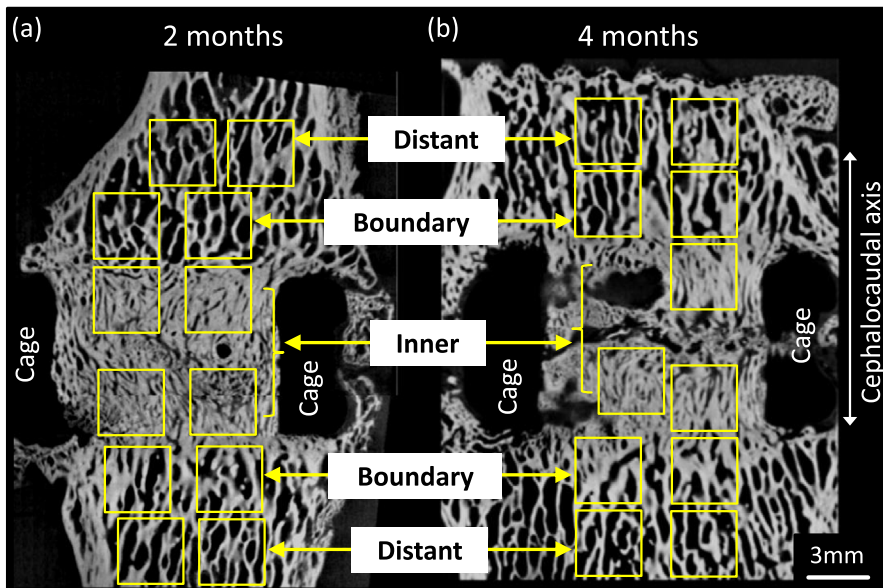

Fig. 5. Sagittal μCT images of sheep vertebral bodies implanted with the open-type intervertebral fusion cages at (a) 2 and (b) 4 months after surgery.
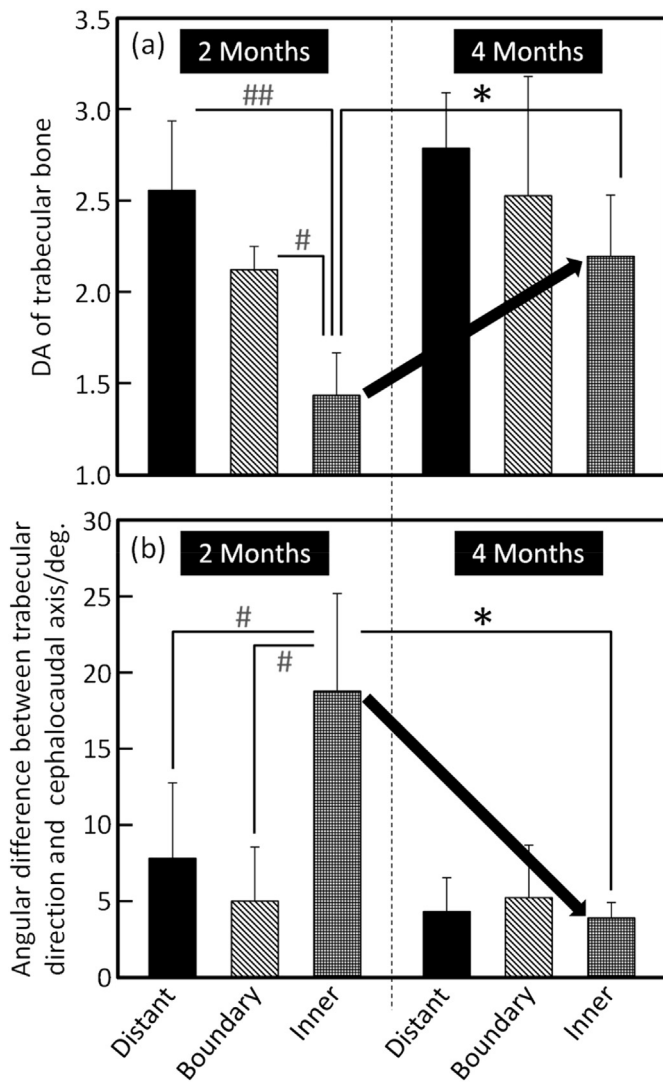
Fig. 7. Variations of trabecular structural anisotropy implanted with the open-type cage. (a) DA of trabecular bone structure and (b) the angular difference between the trabecular aligned direction (direction of the major axis of the fabric ellipse) and the cephalocaudal axis at 2 and 4 months after surgery. $*P < 0.05$ by unpaired t-test. $^#P < 0.05$ by Tukey HSD test.

4.2. Comparison of closed vs. open-type cages: trabecular anisotropy at the bone-cage interface

The mechanical analysis at the bone-cage interface was performed previously by detachment testing (tensile force along the cephalocaudal axis was applied at the interface), demonstrating that the open-type cage had a 1.8- and 1.3-fold higher bonding strength than the closed-type cage at 2 and 4 months postoperatively. For the open-type cage, bonding strength almost doubled between 2 and 4 months [23]. According to our results, the anisotropic trabecular organization possibly contributed to better mechanical performance of the open-type cage. The orientation of collagen has been reported to contribute to the tensile strength and elastic modulus of bone [33,34]. Bone ingrowth into the pores was observed for the closed-type cage with a porous titanium surface coating. However, the trabecular architecture and collagen/apatite arrangement did not orient along the cephalocaudal axis at the interface, which might be one possible reason for the lower bonding strength. To enhance trabecular anisotropy along the loaded direction, pores or grooves that elongate in a specific direction are reportedly effective [21,22]. Thus, there is scope to improve the surface design of closed-type cages.
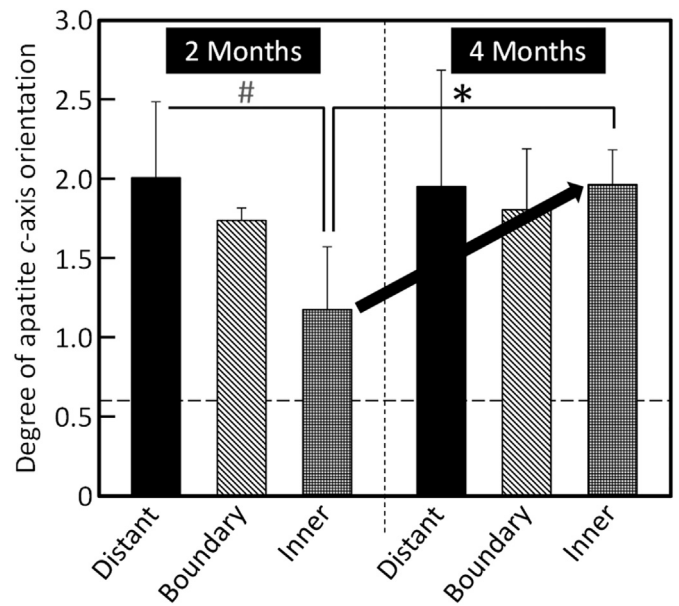

Fig. 8. Variation of the degree of apatite c-axis orientation at 2 and 4 months after surgery. Value for a random apatite orientation is equal to 0.6. $*P < 0.05$ by unpaired t-test. $^#P < 0.05$ by Tukey HSD test.

4.3. Evolution of trabecular anisotropy with implantation duration in the open-type cage

For the open-type cage, a large cavity through the entire thickness of the cage played a role in biologically and structurally connecting the two vertebral bodies beneath the cage. This "through cavity" enabled the growth of bone cells and provided blood vessels supplying oxygen and nutrition and removing waste. The cavity did not intercept the structuralization of bony architecture and stress transfer along the cephalocaudal axis via newly formed bone inside the cavity. The grafted iliac crest with marrow enhanced remodeling and bone reconstruction, which might have led to the onset of stress transfer via the new bone at an early stage postoperatively. The stress transfer along the cephalocaudal axis was evidenced by highly aligned osteocytes in the remodeled trabeculae (Fig. 9d) because osteocytes in the newly formed trabeculae elongated and aligned in accordance with the direction of applied stress [21].

The evolution of trabecular architecture under the anisotropic stress field has been well documented as an architectural adaptation using in vivo models and computational simulations [35]. One example is the rotation of externally loaded, re-oriented trabeculae becoming parallel to the loading axis in order to meet the anisotropic mechanical demand [36,37]. In contrast, an adaptive response through the alteration of material anisotropy, namely the preferential orientation of collagen and apatite in the trabeculae, has been discussed rarely despite its remarkable contribution to Young's modulus [19,34,38] and toughness [20], as demonstrated in cortical bone. It has been reported that cortical bone from several anatomical sites, such as long bones, parietal bones, the mandibles, and lumbar vertebrae, demonstrates preferential orientation of the apatite c-axis in specific directions according to the direction in which the principal stress is applied [18]. When the load is removed from long bones, the material orientation becomes weakened [39]. The insertion of an implant device may alter the stress environment. In many cases, it causes stress shielding. It is important to understand the changes in trabecular anisotropy in response to the alteration of the stress environment because trabecular bone is more likely to be affected by environmental alterations than cortical bone because of its higher turnover activity. The large "through cavity" of the open-type cage used in this study might have maintained the principal stress direction as it was in the intact state. Therefore, new bone between two
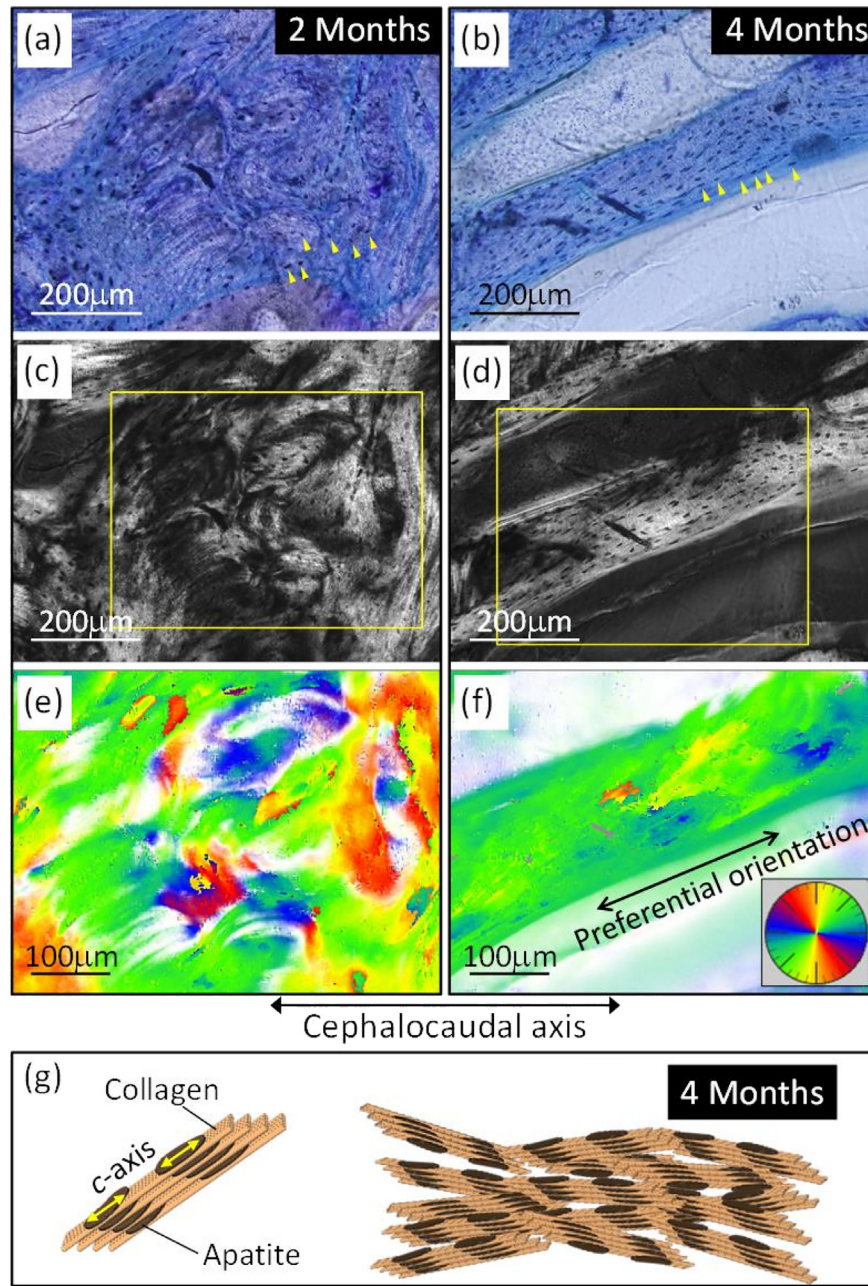
Fig. 9. Histology and collagen orientation at 2 and 4 months after surgery. (a, b) Optical microscope images of the sagittal section stained with hematoxylin & eosin and toluidine blue O and (c, d) polarized images, and (e, f) birefringence images taken from the boxed region in (c) and (d). In (a) and (b), arrowheads indicate osteocytes. Color indication at the right-bottom of (f) shows the slow-axis direction of birefringence representing the preferential collagen orientation direction. (g) Schematic illustration of the preferential collagen/apatite *c*-axis orientation at 4 months after surgery.

vertebral bodies developed structural anisotropy that was similar to the surrounding distant portion. Moreover, other pores that were created on the lateral side contributed to the reduction of stress shielding and the maintenance of the magnitude of the applied stress. It can be said that the open-type cage was effective in achieving a mechanical environment similar to the intact state and the resultant development of anisotropic trabecular features.

Quantitative analyses of trabecular architecture have been performed for the purpose of understanding adaptive responses of trabecular bone to in vivo loading [9]. However, such analyses after the application of implants are relatively scarce [40]. The present study demonstrated that the indices for trabecular anisotropy are meaningful for assessing trabecular health after the implantation of an intervertebral cage. Considering trabecular health, including anisotropy in

trabecular architecture and collagen/apatite orientation may contribute to creating a promising future for the development of bone joint devices. To create trabecular anisotropy, sound stress transfer is crucial; therefore, the shape of a device (e.g., involving pores along a principal stress direction or anisotropically oriented pores/grooves on the implant surface) should be optimized for the controlled in vivo stress transfer.

4.4. Limitations

This study had several limitations. First, we did not include an effective control group. We analyzed a region 3 mm away from the bone-implant boundary to allow comparisons with data from regions just beneath and inside the cage. Non-operated vertebrae would have

been useful as controls. Second, the time points selected for analyses were not sufficient to permit full recovery of trabecular health. Longer implantation duration is preferable in future studies. Third, all analyses were performed in 2D, not 3D. A recently described technique reportedly enables the 3D analysis of trabecular collagen orientation [41]. This will deepen the understanding of bone microstructure and the structure-function relationships of bone materials. Lastly, we did not analyze some important contributors to the mechanical properties of trabecular bone, such as mineral crystallinity [42], collagen cross-linking [43], and so on. The collagen/apatite orientation is possibly closely correlated to such microstructural features. This should be clarified to improve the understanding of trabecular health after the implantation of intervertebral cages. Further studies are needed to validate these points.

5. Conclusions

In the present study, trabecular health was analyzed after the insertion of two types of intervertebral fusion cages into sheep spines. Trabecular health was defined according to the architectural anisotropy and preferential orientation of collagen and apatite in the trabecula. Alterations in trabecular health around the implants differed between the cage types. Moreover, the trabecular health of new bone inside the cage cavity increased with implantation duration, as demonstrated with the open-type cage. The assessment of trabecular anisotropy may be useful for the evaluation of trabecular health and for the validation and refinement of implant designs.

Acknowledgments

Conflict of interest

Manabu Ito has received research grants from HOYA-Pentax, Co., Robert-Reid, Inc. and Century-Medical, Co., and is a board member of AOSpine Knowledge Forum. The other authors declare that they have no conflict of interest.

References

[1] T.H. Smit, The use of a quadruped as an in vivo model for the study of the spine – biomechanical considerations, Eur. Spine J. 11 (2002) 137–144, https://doi.org/10.1007/s005860100346.

[2] T. Pitzen, F.H. Geisler, D. Matthis, H. Müller-Storz, K. Pedersen, W.I. Steudel, The influence of cancellous bone density on load sharing in human lumbar spine: a comparison between an intact and a surgically altered motion segment, Eur. Spine J. 10 (2001), 232C9. https://doi.org/10.1007/s005860000223.

[3] Y. Wang, G. Liu, T. Li, Y. Xiao, Q. Han, R. Xu, Y. Li, Morphometric comparison of the lumbar cancellous bone of sheep, deer, and humans, Comp. Med. 60 (2010) 374–379.

[4] S. Majumdar, M. Kothari, P. Augat, D.C. Newitt, T.M. Link, J.C. Lin, T. Lang, Y. Lu, H.K. Genant, High-resolution magnetic resonance imaging: three-dimensional trabecular bone architecture and biomechanical properties, Bone 22 (1998) 445–454, https://doi.org/10.1016/S8756-3282(98)00030-1.

[5] U.G.K. Wegst, H. Bai, E. Saiz, A.P. Tomsia, R.O. Ritchie, Bioinspired structural materials, Nat. Mater. 14 (2014) 23–36, https://doi.org/10.1038/nmat4089.

[6] S.D. Rockoff, E. Sweet, J. Bleustein, The relative contribution of trabecular and cortical bone to the strength of human lumbar vertebrae, Calcif. Tissue Res. 3 (1969) 163–175, https://doi.org/10.1007/BF02058659.

[7] R. Andresen, H.J. Werner, H.C. Schober, Contribution of the cortical shell of vertebrae to mechanical behavior of the lumbar vertebrae with implications for predicting fracture risk, Br. J. Radiol. 71 (1998) 759–765, https://doi.org/10.1259/bjr.71.847.9771387.

[8] S.K. Eswaran, A. Gupta, M.F. Adams, T.M. Keaveny, Cortical and trabecular load sharing in the human vertebral body, J. Bone Miner. Res. 21 (2006) 307–314, https://doi.org/10.1359/jbmr.2006.21.2.307.

[9] K. Tsubota, Y. Suzuki, T. Yamada, M. Hojo, A. Makinouchi, T. Adachi, Computer simulation of trabecular remodeling in human proximal femur using large-scale voxel FE models: approach to understanding Wolff's law, J. Biomech. 42 (2009) 1088–1094, https://doi.org/10.1016/j.jbiomech.2009.02.030.

[10] F.F. Sabry, N.A. Ebraheim, J.N. Mehalik, A.T. Rezcallah, Internal architecture of the calcaneus: implications for calcaneus fractures, Foot Ankle Int. 21 (2000) 114–118, https://doi.org/10.1177/107110070002100204.

[11] Y.N. Yeni, B. Wu, L. Huang, D. Oravec, Mechanical loading causes detectable changes in morphometric measures of trabecular structure in human cancellous bone, J. Biomech. Eng. 135 (2013), 054505. https://doi.org/10.1115/1.4024136.

[12] J.H. Kinney, J.S. Stölken, T.S. Smith, J.T. Ryaby, N.E. Lane, An orientation distribution function for trabecular bone, Bone 36 (2005) 193–201, https://doi.org/10.1016/j.bone.2004.09.023.

[13] X.S. Liu, X.H. Zhang, X.E. Guo, Contributions of trabecular rods of various orientations in determining the elastic properties of human vertebral trabecular bone, Bone 45 (2009) 158–163, https://doi.org/10.1016/j.bone.2009.04.201.

[14] S. Miyabe, T. Nakano, N. Takano, T. Adachi, H. Iwaki, A. Kobayashi, K. Takaoka, Y. Umakoshi, Two-dimensional quantitative analysis of preferential alignment of BAp c-axis for isolated human trabecular bone using microbeam X-ray diffractometer with a transmission optical system, Mater. Trans. 48 (2007) 343–347, https://doi.org/10.2320/matertrans.48.343.

[15] E. Rokita, P. Chevallier, P.H.A. Mutsaers, Z. Tabor, A. Wróbel, Studies of crystal orientation and calcium distribution in trabecular bone, Nucl. Inst. Methods Phys. Res. B 240 (2005) 69–74, https://doi.org/10.1016/j.nimb.2005.06.089.

[16] M. Georgiadis, M. Guizar-Sicairos, O. Gschwend, P. Hangartner, O. Bunk, R. Müller, P. Schneider, Ultrastructure organization of human trabeculae assessed by 3D sSAXS and relation to bone microarchitecture, PLoS ONE 11 (2016), e0159838. https://doi.org/10.1371/journal.pone.0159838.

[17] J.Y. Rho, M.E. Roy, T.Y. Tsui, G.M. Pharr, Elastic properties of microstructural components of human bone tissue as measured by nanoindentation, J. Biomed. Mater. Res. 45 (1999) 48–54, https://doi.org/10.1002/(SICI)1097-4636(199904)45:1<48::AID-JBM7>3.0.CO;2-5.

[18] T. Nakano, K. Kaibara, Y. Tabata, N. Nagata, S. Enomoto, E. Marukawa, Y. Umakoshi, Unique alignment and texture of biological apatite crystallites in typical calcified tissues analyzed by microbeam X-ray diffractometer system, Bone 31 (2002) 479–487, https://doi.org/10.1016/S8756-3282(02)00850-5.

[19] T. Ishimoto, T. Nakano, Y. Umakoshi, Y. Ymamoto, Y. Tabata, Degree of biological apatite c-axis orientation rather than bone mineral density controls mechanical function in bone regenerated using recombinant bone morphogenetic protein-2, J. Bone Miner. Res. 28 (2013) 1170–1179, https://doi.org/10.1002/jbmr.1825.

[20] S. Li, E. Demirci, V.V. Silberschmid, Variability and anisotropy of mechanical behavior of cortical bone in tension and compression, J. Mech. Behav. Biomed. Mater. 21 (2013) 109–120, https://doi.org/10.1016/j.jmbbm.2013.02.021.

[21] Y. Noyama, T. Nakano, T. Ishimoto, T. Sakai, H. Yoshikawa, Design and optimization of the oriented groove on the hip implant surface to promote bone microstructure integrity, Bone 52 (2013) 659–667, https://doi.org/10.1016/j.bone.2012.11.005.

[22] S. Kuroshima, T. Nakano, T. Ishimoto, M. Sasaki, M. Inoue, M. Yasutake, T. Sawase, Optimally oriented grooves on dental implants improves bone quality around implants under repetitive mechanical loading, Acta Biomater. 48 (2017) 433–444, https://doi.org/10.1016/j.actbio.2016.11.021.

[23] K. Yamada, M. Ito, T. Akazawa, M. Murata, T. Yamamoto, N. Iwasaki, A preclinical large animal study on a novel intervertebral fusion cage covered with high porosity titanium sheets with a triple pore structure used for spinal fusion, Eur. Spine J. 24 (2015) 2530–2537, https://doi.org/10.1007/s00586-015-4047-2.

[24] A. Abbushi, M. Čabraja, U.W. Thomale, C. Woiciechowsky, S.N. Kroppenstedt, The influence of cage positioning and cage type on cage migration and fusion rates in patients with monosegmental posterior lumbar interbody fusion and posterior fixation, Eur. Spine J. 18 (2009) 1621–1628, https://doi.org/10.1007/s00586-009-1036-3.

[25] K. Kato, A. Yamamoto, S. Ochiai, Y. Daigo, T. Isobe, S. Matano, K. Omori, Cell proliferation, corrosion resistance and mechanical properties of novel titanium foam with sheet shape, Mater. Trans. 53 (2012) 724–732, https://doi.org/10.2320/matertrans.M2011325.

[26] M. Ito, Y. Kotani, Y. Hojo, K. Abumi, T. Kadosawa, A. Minami, Evaluation of hydroxyapatite ceramic vertebral spacers with different porosities and their binding capability to the vertebral body: an experimental study in sheep, J. Neurosurg. Spine 6 (2007) 431–437, https://doi.org/10.3171/spi.2007.6.5.431.

[27] E.M. Lindley, C. Barton, T. Blount, E.L. Burger, C.M. Cain, H.B. Seim 3rd, A.S. Turner, V.V. Patel, An analysis of spine fusion outcomes in sheep pre-clinical models, Eur. Spine J. 26 (2017) 228–239, https://doi.org/10.1007/s00586-016-4544-y.

[28] S.C. Cowin, The relationship between the elasticity tensor and the fabric tensor, Mech. Mater. 4 (1985) 137–147, https://doi.org/10.1016/0167-6636(85)90012-2.

[29] N. Ugryumova, S.V. Gangnus, S.J. Matcher, Three-dimensional optic axis determination using variable-incidence-angle polarization-optical coherence tomography, Opt. Lett. 31 (2006) 2305–2307, https://doi.org/10.1364/OL.31.002305.

[30] A. Sekita, A. Matsugaki, T. Ishimoto, T. Nakano, Synchronous disruption of anisotropic arrangement of the osteocyte network and collagen/apatite in melanoma bone

metastasis, J. Struct. Biol. 197 (2017) 260–270, https://doi.org/10.1016/j.jsb.2016.12.003.

[31] H.J. Wilke, A. Kettler, K.H. Wenger, L.E. Claes, Anatomy of the sheep spine and its comparison to the human spine, Anat. Rec. 247 (1997) 542–555, https://doi.org/10.1002/(SICI)1097-0185(199704)247:4<542::AID-AR13>3.0.CO;2-P.

[32] H.J. Wilke, A. Kettler, L. Cleas, Are sheep spines a valid model for human spines? Spine 22 (1997) 2365–2374, https://doi.org/10.1097/00007632-199710150-00009.

[33] R.B. Martin, J. Ishida, The relative effects of collagen fiber orientation, porosity, density, and mineralization on bone strength, J. Biomech. 22 (1989) 419–426, https://doi.org/10.1016/0021-9290(89)90202-9.

[34] A. Ascenzi, E. Bonucci, The tensile properties of single osteons, Anat. Rec. 158 (1967) 375–386, https://doi.org/10.1002/ar.1091580403.

[35] T.L. Kivell, A review of trabecular bone functional adaptation: what have we learned from trabecular analyses in extant hominoids and what can we apply to fossils? J. Anat. 228 (2016) 569–594, https://doi.org/10.1111/joa.12446.

[36] R. Huiskes, R. Ruimerman, G.H. van Lenthe, J.D. Janssen, Effects of mechanical forces on maintenance and adaptation of form in trabecular bone, Nature 405 (2000) 704–706, https://doi.org/10.1038/35015116.

[37] M.M. Barak, D.E. Lieberman, J.J. Hublin, A Wolff in sheep's clothing: trabecular bone adaptation in response to changes in joint loading orientation, Bone 49 (2011) 1141–1151, https://doi.org/10.1016/j.bone.2011.08.020.

[38] M.G. Ascenzi, A. Benvenuti, A. Ascenzi, Single osteon micromechanical testing, in: Y.H. An, R.A. Draughn (Eds.), Mechanical Testing of Bone and the Bone-Implant Interface, Boca Raton, CRC Press, 2000.

[39] J. Wang, T. Ishimoto, T. Nakano, Unloading-induced degradation of the anisotropic arrangement of collagen/apatite in rat femurs, Calcif. Tissue Int. 100 (2017) 87–94, https://doi.org/10.1007/s00223-016-0200-0.

[40] R.E. Guldberg, M. Richards, N.J. Caldwell, C.L. Kuelske, S.A. Goldstein, Trabecular bone adaptation to variations in porous-coated implant topology, J. Biomech. 30 (1997) 147–153, https://doi.org/10.1016/S0021-9290(96)00106-6.

[41] M. Georgiadis, M. Guizar-Sicairos, A. Zwahlen, A.J. Trüssel, O. Bunk, R. Müller, P. Schneider, 3D scanning SAXS: a novel method for the assessment of bone ultra-structure orientation, Bone 71 (2015) 42–52, https://doi.org/10.1016/j.bone.2014.10.002.

[42] A.H. Ng, S. Omelon, F. Variola, B. Allo, T.L. Willett, B.A. Alman, M.D. Grynpas, Ady-namic bone decreases bone toughness during aging by affecting mineral and matrix, J. Bone Miner. Res. 31 (2016) 369–379, https://doi.org/10.1002/jbmr.2702.

[43] M. Saito, Y. Kida, T. Nishizawa, S. Arakawa, H. Okabe, A. Seki, K. Marumo, Effects of 18-month treatment with bazedoxifene on enzymatic immature and mature cross-links and non-enzymatic advanced glycation end products, mineralization, and trabecularmicroarchitecture of vertebra in ovariectomized monkeys, Bone 81 (2015) 573–580, https://doi.org/10.1016/j.bone.2015.09.006.